Hierarchical nanostructured conducting polymer hydrogel with high electrochemical activity

Lijia Pan[a,b,1], Guihua Yu[b,1], Dongyuan Zhai[a], Hye Ryoung Lee[c], Wenting Zhao[d], Nian Liu[e], Huiliang Wang[d], Benjamin C.-K. Tee[c], Yi Shi[a], Yi Cui[d,f,2], and Zhenan Bao[b,2]

[a]National Laboratory of Microstructures (Nanjing), School of Electronic Science and Engineering, Nanjing University, Nanjing 210093, China; [b]Department of Chemical Engineering, Stanford University, Stanford, CA 94305; [c]Department of Electrical Engineering, Stanford University, Stanford, CA 94305; [d]Department of Materials Science and Engineering, Stanford University, Stanford, CA 94305; [e]Department of Chemistry, Stanford University, Stanford, CA 94305; and [f]Stanford Institute for Materials and Energy Sciences, SLAC National Accelerator Laboratory, 2575 Sand Hill Road, Menlo Park, CA 94025

Conducting polymer hydrogels represent a unique class of materials that synergizes the advantageous features of hydrogels and organic conductors and have been used in many applications such as bioelectronics and energy storage devices. They are often synthesized by polymerizing conductive polymer monomer within a nonconducting hydrogel matrix, resulting in deterioration of their electrical properties. Here, we report a scalable and versatile synthesis of multifunctional polyaniline (PAni) hydrogel with excellent electronic conductivity and electrochemical properties. With high surface area and three-dimensional porous nanostructures, the PAni hydrogels demonstrated potential as high-performance supercapacitor electrodes with high specific capacitance ($\sim$480 F·g^{-1}), unprecedented rate capability, and cycling stability ($\sim$83% capacitance retention after 10,000 cycles). The PAni hydrogels can also function as the active component of glucose oxidase sensors with fast response time ($\sim$0.3 s) and superior sensitivity ($\sim$16.7 μA·mM^{-1}). The scalable synthesis and excellent electrode performance of the PAni hydrogel make it an attractive candidate for bioelectronics and future-generation energy storage electrodes.

conductive polymer hydrogel | supercapacitors | biosensors

Hydrogels are polymeric networks that have a high level of hydration and three-dimensional (3D) microstructures bearing similarities to natural tissues (1, 2). Hydrogels based on conducting polymers [e.g., polythiophene, polyaniline (PAni), and polypyrrole] combine the unique properties of hydrogels with the electrical and optical properties of metals or semiconductors (3–6) thus offering an array of features such as intrinsic 3D microstructured conducting frameworks that promote the transport of charges, ions, and molecules (7). Conducting polymer hydrogels provide an excellent interface between the electronic-transporting phase (electrode) and the ionic-transporting phase (electrolyte), between biological and synthetic systems, as well as between soft and hard materials (8). As a result, conducting polymer hydrogels have demonstrated great potential for a broad range of applications from energy storage devices such as biofuel cells and supercapacitors, to molecular and bioelectronics (9) and medical electrodes (8).

To date, the synthetic routes toward conducting polymer hydrogels include synthesizing a conducting polymer monomer within a nonconducting hydrogel matrix (8, 9) using multivalent metal ions (Fe^{3+} or Mg^{2+}) to crosslink poly(3,4-ethylenedioxythiophene)-poly(styrenesulfonate) (PEDOT:PSS) (10, 11) and using nonconducting poly(ethylene glycol) diglycidyl ether, or poly(styrenesulfonate) to crosslink PAni (12, 13); however, nonconducting hydrogel matrix and polymers result in the deterioration of the electrical properties, whereas excessive metal ions may reduce the biocompatibility of hydrogels. Moreover, there have yet been any reports in regard to conductive hydrogels that can be facilely micropatterned, which is important for fabricating hydrogel-based electronic devices. Hence, a big challenge still remains to synthesize polymer hydrogels that exhibit facile processability, excellent electronic property, and high electrochemical activity.

In this article, we used phytic acid (an abundant natural product found in plants) (14, 15) as the gelator and dopant to directly form a conducting polymer network free of insulating polymers. The PAni hydrogels with phytic acid gelator showed a new record conductivity of 0.11 S·cm^{-1} among several conducting polymer hydrogels reported to date. Furthermore, it also possesses excellent processability because they can be ink-jet printed or spray coated through stencil masks into various desired micropatterns. The highly hierarchical structure and good electrical conductivity of the hydrogel render them as high performance supercapacitor electrodes with high capacitance, unprecedented rate capability, and cycling stability. They can also be used as glucose enzyme sensors with high sensing speed and sensitivity. This is the first described conducting polymer hydrogel that has exhibited high electronic property and superior electrode performance.

Results and Discussion

The gelation mechanism of PAni hydrogel is illustrated in Fig. 1*A*. Phytic acid reacts with PAni by protonating the nitrogen groups on PAni. Because each phytic acid molecule can interact with more than one PAni chain, this crosslinking effect results in the formation of a mesh-like hydrogel network (Fig. 1*A*). Note that mesh size is often used to describe the structure of crosslinked hydrogel, which is defined as the correlation length between two adjacent crosslinks and indicates the space available between the macromolecular chains (7). In a typical synthesis, a solution containing the oxidative initiator (solution A) was mixed with a solution containing the aniline monomer and phytic acid (solution B). With the polymerization of PAni, we observed a change in the color of the solution from light brown (color of phytic acid) to dark green (color of emeraldine PAni). The mixed solution typically gelates in approximately 3 min (Fig. 1*B*) consistent with in situ open-circuit potentials (*SI Appendix*, Fig. S1). That indicates that the polymerization is near completion in 3 min. After removing excessive ions and purification through extensive rinsing with deionized (DI) water, the PAni hydrogel was subsequently swollen and its water content was measured to be 92.6% (wt/wt) by lyophilization, and 93% (wt/wt) by thermogravimetry (TGA) (*SI Appendix*, Fig. S2). This synthetic approach is highly versatile as it offers great tunability. The PAni hydrogel can be
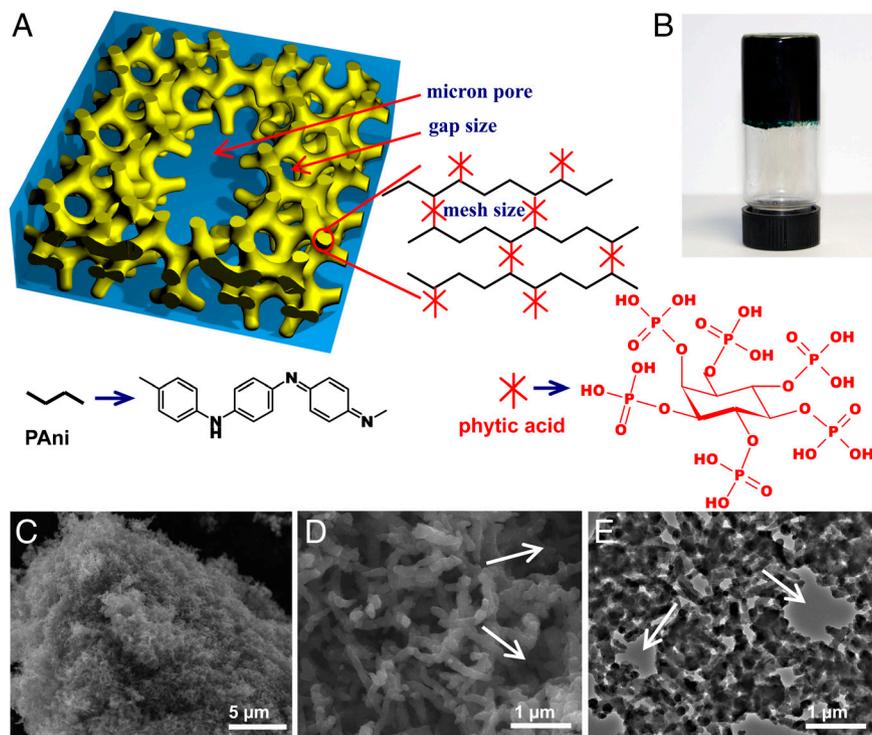
Fig. 1. Chemical structure and morphological characterization of phytic acid gelated and doped polyaniline hydrogel. (*A*) Schematic illustrations of the 3D hierarchical microstructure of the gelated PAni hydrogel where phytic acid plays the role as a dopant and a crosslinker. Three levels of hierarchical porosity from angstrom, nanometer to micron size pores have been highlighted by red arrows. (*B*) A photograph of the PAni hydrogel inside a glass vial. (*C*) SEM image of a piece of dehydrated hydrogel. (*D*) A higher magnification SEM image showing the interconnected network of dendritic PAni nanofibers. (*E*) A TEM image showing the continuous nanostructured network of the dehydrated PAni hydrogel. The white arrows in *D* and *E* denote the micron size pores in PAni hydrogel.

formed in a wide range of molar ratios of aniline monomer to phytic acid between 2 : 1 and 7 : 1, and with other oxidative initiators such as ammonium cerous sulphate and hydrogen peroxide with trace iron trichloride catalyst. The PAni hydrogel can also be synthesized by a biphasic reaction. For example, placing the aniline monomer in a chloroform phase with phytic acid and the initiator in the aqueous phase produced dark green PAni at the interface that gradually diffused into the aqueous phase and formed PAni hydrogel in the aqueous phase finally (*SI Appendix*, Fig. S3).

The chemical structure of the hydrogel was analyzed by FTIR and UV-visible (UV-vis) spectroscopy and is observed to be identical to that of acid doped emeraldine PAni salt (*SI Appendix*). The FTIR spectrum of phytic acid doped PAni indicates that it is the emeraldine salt form of PAni with two characteristic peaks located at 1,570 and 1,480 cm^{-1} corresponding to the stretching vibration of the quinoid ring and benzenoid ring (16, 17), respectively. The state of these products was emeraldine rather than solely leucoemeraldine or permigraniline (*SI Appendix*, Fig. S4). The UV-vis spectrum of the PAni showed a band at 440 nm and a long tail at $\lambda > 800$ nm. These features are consistent with the doped emeraldine state of PAni (*SI Appendix*, Fig. S5). The conductivity of the wet PAni hydrogel is about 0.11 S·cm^{-1} at 298 K by measuring the impedance between two platinum electrodes at a frequency range of 0.01 Hz ∼ 100 KHz (*SI Appendix*, Fig. S6), which is the highest reported value for conducting polymer hydrogels (typically in the range of 0.1–10 mS·cm^{-1}) (18, 19). The temperature dependence of conductivity of the dried powder of the PAni hydrogel (pressed into pellet) was studied by a standard four-point-probe method. The electronic conductivity was measured to be 0.23 S·cm^{-1} at room temperature. The conductivity of the phytic acid doped PAni increased with the decreasing temperature between 20 and 80 K (*SI Appendix*, Fig. S7) showing a metallic behavior. Between 80 and 300 K, the conductivity decreased with the decreasing temperature exhibiting typical semi-

conductor behavior (*SI Appendix*, Fig. S8). The temperature dependence of conductivity is consistent with the 1D variable range hopping (1D-VRH) model previously proposed by Mott (20) (*SI Appendix*).

SEM images (Fig. 1 *C* and *D*) show the 3D porous foam morphology of the dehydrated PAni hydrogel. The foam-like nanostructures are constructed with coral-like dendritic nanofibers with uniform diameters of 60–100 nm. Further investigation by transmission electron microscopy (TEM) reveals that the PAni forms a continuous network (Fig. 1*E*). Two levels of pores were observed in the TEM and SEM images. The first level was the pores between the branched nanofibers (the average gap size), and the second level was the bigger micron size pores marked by the white arrows in Fig. 1 *D* and *E*. The Brunauer–Emmett–Teller (BET) specific surface area of the dehydrated hydrogel was measured to be 41.6 m^2·g^{-1} (*SI Appendix*, Fig. S9), which was comparable with other chemically synthesized PAni nanofibers.

The facile synthesis route of our PAni hydrogels provides a practical method to bulk synthesis of monolithic porous 3D nanostructures. Such 3D interconnected PAni nanofiber structures can be more effective than wires and particles for sensing and electrochemical device applications due to large open channels of the micron-scale and nanometer-scale pores within the structures (21). Nanoscale interconnected conducting matrix and porosities offer greater effective surface areas than bulk materials and facilitate the transport of electrons and ions (22, 23). The 3D framework is stable and sustains from the change in its water content or the dedoping process against ammonia solution because of the rigidity of the PAni main chains and interconnected frame structure.

Moreover, the swelling nature of PAni hydrogel offers additional effective surface areas between molecular chains and the solution phase (Fig. 1*A*) as well as the enhanced conductivity of PAni. For our PAni hydrogel, the additional interface between the PAni chain and the solution phase is created when it is swollen in

water and further facilitates electron transport and easy access of electrolyte ions within the hierarchical 3D structures of the PAni electrodes. The structural difference between the swollen PAni hydrogel and the dehydrated PAni was studied by atomic force microscopy (AFM) and X-ray diffraction (XRD). The AFM images showed that the fully swollen PAni hydrogel had nanofibers about 200–300 nm in diameter compared to 60–100 nm in the dehydrated state (*SI Appendix*, Fig. S10). XRD pattern indicates that the swelling increased the distance between polymer chains (*SI Appendix*, Fig. S11).

The swelling structures of the PAni hydrogel may allow for the permeation of ions and small molecules in between PAni chains leading to high performance of electrochemical devices. Moreover, it is found that swollen PAni hydrogel has decreased the $\pi-\pi$ stacking distance from 3.56 to 3.18 Å (*SI Appendix*) that may result from reduced distortion of PAni chains and increased mobility of chain segment. For organic conductors, it is well known that cofacially stacked conjugated backbones (the $\pi-\pi$ stacking distance) greatly influence electron orbital overlap and, therefore, the conductivity (24). With the above observation, we conclude that the decreased $\pi-\pi$ stacking distance leads to the high conductivity of our hydrogel samples.

The phytic acid plays a critical role in the gelation, microstructure formation, and surface property modification of the PAni hydrogel. Phytic acid crosslinked PAni by protonating the nitrogens on PAni chains (namely the amine and imine groups). Protonation of the imine groups renders the PAni conducting and is thus considered a way to dope PAni (25). In contrast to the doping of inorganic semiconductors with trace impurity atoms, a large amount of dopant is usually needed for organic conductors, and the degree of protonation is correlated to the pH of solution (25). The phytic acid renders the PAni hydrogel hydrophilic because there is an excess of phosphorous groups. This results in a high level of hydration and is critical for the formation of hydrogel. We measured the contact angle of the phytic acid doped PAni to be ~24° while the contact angles for the sulfuric acid doped PAni and the phosphorus acid doped PAni are observed to be 69° and 54°, respectively (*SI Appendix*, Fig. S12). Even when the hydrogel is dehydrated, it can be readily rehydrated (*SI Appendix*, Fig. S13). The molecular structure of phytic acid crosslinking PAni favors the formation of dendritic nanofibers and the interconnected microstructures of PAni hydrogel because each phytic acid molecule is able to interact with several PAni chains to result in branched microstructures.

Our developed chemistry to synthesize PAni hydrogel also offers scalability in its processing. It can be ink-jet printed or micropatterned by spray coating through stencil masks, which is important for device fabrication *en masse* (26). From the perspective of the fabrication process, highly scalable approaches, e.g., facile solution-based process and printing technique to make functional electrodes and construct electrochemical devices such as biosensor arrays and supercapacitors are important. For instance, we have recently investigated solution-based coating and printing techniques to make conductive carbon nanotubes (CNTs)-based papers and textiles as electrodes and/or current collectors for batteries and supercapacitors (27).

When printing polymers, ink-jet printing is often hampered by the limited solubility and high viscosity of polymer solutions. In our experiments, it was observed that direct printing of hydrogel materials caused the nozzle to clog. We overcame this difficulty by sequentially depositing two distinct solutions onto the substrate. Briefly, we first printed a solution A containing the oxidative initiator followed by printing a second solution that contained the phytic acid and the aniline monomer. The patterned PAni hydrogel was formed where solutions A and B are able to interact (Fig. 2 *A–C*). The viscosity of the solutions is suitable for ink-jet printing and allows direct deposition without the need for additives (*SI Appendix*, Table S1). SEM images indicate that the
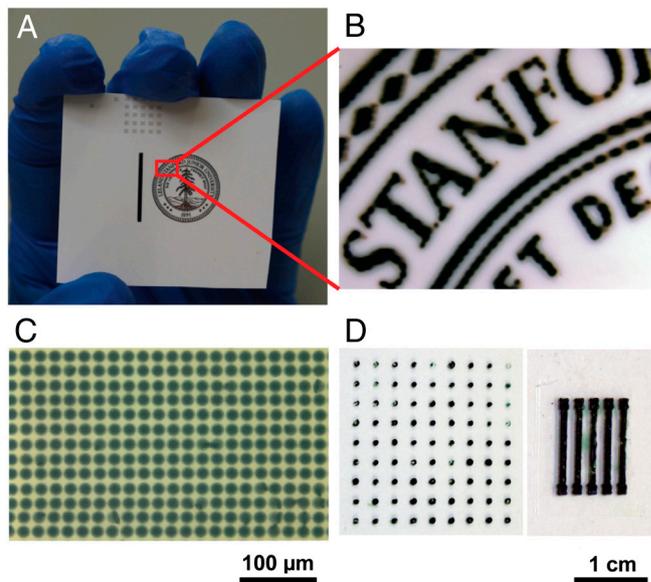

Fig. 2. Micropatterning of PAni hydrogel by ink-jet printing (*A–C*) and spray coating (*D*). (*A*) Photographs of an ink-jet-printed image on a piece of glossy photo paper. (*B*) The magnified image. (*C*) Optical micrograph of ink-jet printed hydrogel dot array with the diameter of each dot about 18 μm. (*D, Left*) A dot array of PAni hydrogels generated by mask-spray coating with dot diameter about 1 mm. (*Right*) An electrode array of PAni hydrogel produced by mask-spray coating with line width about 2 mm.

morphologies of both the ink-jet-printed hydrogels are similar to the bulk hydrogels (*SI Appendix*, Fig. S14). Fig. 2*C* shows a microdot array with diameters of ~18 μm of PAni hydrogel printed with a 9 μm nozzle. A 21.5 μm nozzle produces an array of microdots of 40 μm diameter. For electrode fabrication, ink-jet printing has the advantages of high precision, fine patterns, and suitability for large area patterning (28).

In addition, spray coating is another effective deposition method that is able to produce patterns using shadow masks with low cost; however, it is more difficult to obtain as good pattern resolution as ink-jet printing. For our hydrogel, micropatterns of millimeter size can be produced by spray coating two solutions (solutions A and B) alternatively multiple times through poly (dimethylsiloxane) (PDMS) soft stencil masks (Fig. 2*D*). Such stencil lithography technique provides a unique high-throughput shadow mask method allowing parallel resistless patterning of PAni hydrogel onto a range of substrates. The PAni hydrogels resulting from our described approach would lead to highly conductive, large-area patterned microelectrodes potentially useful for supercapacitors, lithium batteries, biosensors, chemical sensors, and other bioelectrodes.

The 3D hierarchical porous nanostructure of PAni hydrogel resulted in the superior performance of our fabricated electrochemical devices. Basically, all electrochemical systems involve ionic and electronic transport processes at the interface between the electrode and the electrolyte solution. A larger interfacial area can lead to more efficient electrochemical processes. For pseudocapacitive electrode materials such as conducting polymers, the pseudocapacitance stems from the faradic reactions (the doping and undoping processes) that occur near the surface of active electrode materials. Our 3D hierarchical nanostructured hydrogels can provide a relatively short diffusion path for electrolyte ions to access the electroactive surface of PAni thus improving the electrochemical use of active materials (29).

To evaluate the electrochemical performance of the PAni hydrogels as active supercapacitor electrodes, we performed a combination of electrochemical impedance spectroscopy (EIS), cyclic voltammetry (CV), and galvanostatic charge-discharge
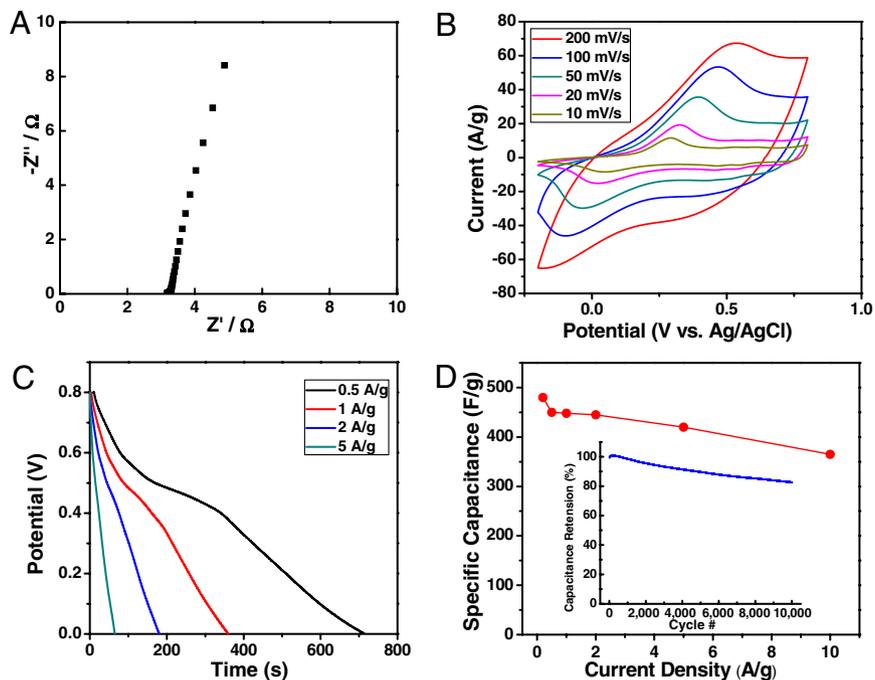
Fig. 3. PAni hydrogel as high-performance 3D nanostructured electrodes for supercapacitors. (A) Impedance curve of a PAni hydrogel-based supercapacitor electrode. (B) Cyclic voltammogram curves of the PAni hydrogel electrode at different scan rates (10–200 mV·s^{-1}). (C) Galvanostatic discharge profiles at various current densities (0.5–5 A·g^{-1}). (D) Summary plot of specific capacitance values vs. current density for PAni hydrogel-based electrodes. (Inset) Cycling test showing ~83% capacitance retention over 10,000 cycles at high current rate of 5 A·g^{-1}.

measurements in a conventional three-electrode system. Fig. 3A shows the impedance curve of PAni hydrogel based electrodes measured in a 1 M H$_2$SO$_4$ electrolyte. The equivalent series resistance (ESR) extracted from high frequency (100 kHz) is estimated to be ~3.2 Ω, which is a small value for a PAni mass loading of 2 mg·cm^{-2} (dry weight of PAni). The nearly vertical shape of the obtained curve at lower frequencies indicates an ideal capacitive behavior of the electrodes. Moreover, the charge transfer resistance read from the small size of the semicircle (<0.1 Ω) is remarkably small suggesting favorable ion transport within the 3D continuous nanostructured framework. Fig. 3B shows the rate-dependent CVs with the potential window of −0.2 to 0.8 V vs. Ag/AgCl reference electrode at scan rates of 10, 20, 50, 100, and 200 mV·s^{-1}. The typical PAni redox peaks are clearly seen (30). Galvanostatic charge-discharge measurements were also taken at various current densities. Fig. 3C shows the discharge profiles for the hydrogel electrodes at current densities of 0.5, 1, 2, and 5 A·g^{-1}. The corresponding specific capacitance values vs. scan rates from discharge curves based on the total mass of active PAni hydrogel materials (dry weight) as summarized in Fig. 3D yielded a specific capacitance of ~480 F·g^{-1} at current density of 0.2 A·g^{-1}.

In addition, our PAni hydrogel based electrodes yielded excellent rate performance with only ~7% capacitance loss when current density was increased by a factor of 10 (e.g., ~450 F·g^{-1} at 0.5 A·g^{-1} decreased to ~420 F·g^{-1} at 5 A·g^{-1}) indicating an exceptional rate capability for high power performance. This is in sharp contrast to previously reported PAni-based electrodes, where a typical 25–40% capacitance loss was seen at high power (31–34). We attribute the high rate performance to the facile electronic and ionic transport stemming from the hierarchically conductive network discussed above. Moreover, as the mass loading was increased to 5 mg·cm^{-2}, the PAni hydrogel electrodes still retained a high capacitance performance (specific capacitance of ~460 F·g^{-1} at 0.2 A·g^{-1}) as well as an excellent rate capability (~92% capacitance retention when current density was increased from 0.5 A·g^{-1} to 5 A·g^{-1}, *SI Appendix,* Fig. S15). The areal capacitance for this high loading reached a maximum value of

2.3 F·cm^{-2}, which is higher than those reported previously for PAni-based supercapacitor devices (between 0.9 to 1.8 F·cm^{-2}) (30, 34).

In addition, PAni hydrogel-based electrodes also exhibited good cycling stability, which is another key requirement in the operation of supercapacitors. Conducting polymers-based supercapacitors often suffer from limited cyclability due to swelling and shrinking of electroactive polymers during its charging and discharging processes (29). The cycling performance of our 3D nanostructured hydrogel electrodes showed capacitance retention as high as ~91% over 5,000 cycles and ~83% retention over 10,000 cycles at a high current density of 5 A·g^{-1}, which is superior to the PAni-based supercapacitors reported in previous work (typically 60 ~ 85% retention for over 1,000 cycles) (31, 35). The superior cycling performance achieved in our hydrogel electrode system confirms the unique advantages of the highly porous interconnected nanostructures and phytic acid crosslinked conducting polymer hydrogels that can accommodate the swelling and shrinking of the polymer network during intensive cycling processes.

The high surface area and interconnected conducting polymer hydrogels are also attractive features for high-performance chemical and biological sensing. As a proof-of-concept, the PAni hydrogels were fabricated as enzyme glucose sensors. The working mechanism of the sensor is based on the redox properties of the glucose oxidase (GOx) where the enzymatic reaction of GOx and glucose is monitored via electrochemical measurement of the GOx-PAni hydrogel electrode (36). A two-compartment, three-electrode cell was employed for the glucose sensing test. It was equipped with a platinum electrode and a SCE that functions as the counter electrode and reference electrode, respectively. The electrocatalytic features of GOx were evaluated by voltammetry.

It was observed that the current change of the PAni hydrogel was linearly correlated to the amount of glucose added into the buffer solution (within the concentration range of 0.1–2.6 mM with a correlation coefficient of 0.9998, see Fig. 4 A and B). Upon addition of increasing concentration of glucose, the observed
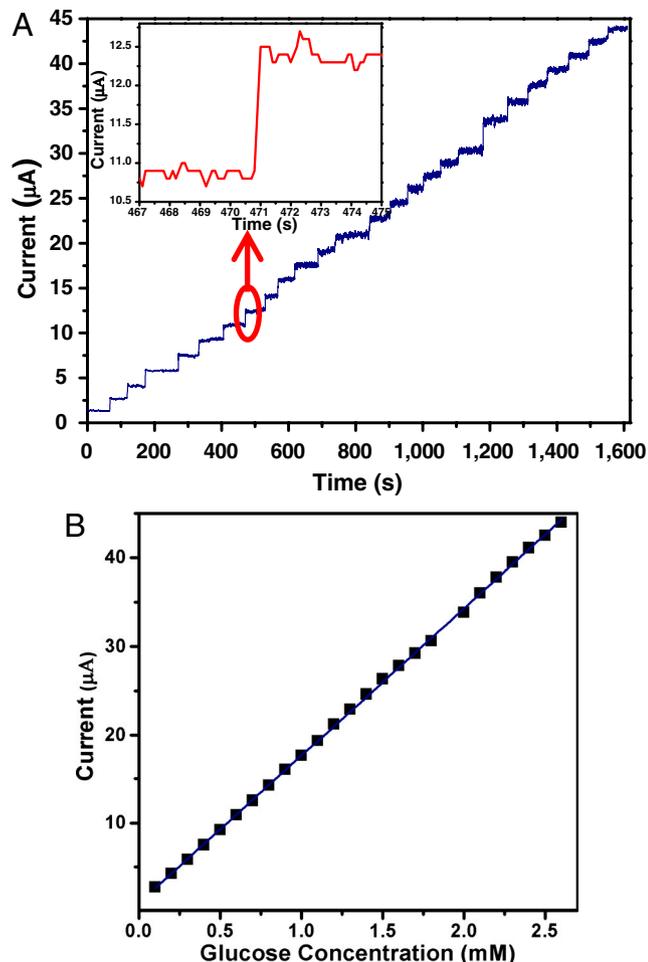
Fig. 4. PAni hydrogel as high-performance 3D nanostructured electrode for glucose enzyme sensor. (*A*) Amperometric response of the GOx-PAni hydrogel-based enzymatic biosensor to successive addition of glucose in PBS (0.1 M, pH 5.5); the concentration of glucose was increased 0.1 mM for each time (increased 0.2 mM at 1,180 s). *Inset* shows a magnification of the seventh additions of glucose. (*B*) The corresponding calibration plot showing nearly linear amperometric response vs. glucose concentration.

current as measured by the PAni hydrogel electrode rapidly increased until a plateau is reached (Fig. 4*A*). Furthermore, the obtained response time was ~0.3 s (Fig. 4*A*, *Inset*, 95% of steady-state current) with an average sensing time of ~1.1 s, which rivals the performance of the fastest reported response time (~0.2 s) of glucose sensor made with a single PAni nanojunction (37), and superior to that based on PAni nanotube array (~3 s) (38). The sensitivity of our PAni hydrogel glucose sensor is 16.7 μA· mM^{-1}, and the sensitivity per unit area is 85.4 μA·mM^{-1}· cm^{-2}, which are higher than the reported glucose sensors based on other PAni nanostructures (37), polypyrrole (39), carbon nanotubes (40), and single walled carbon nanotubes (41). The exceptionally fast response and high sensitivity are again attributed to the relatively short diffusion path (thus favoring molecular and electronic transport) that is due to the open channels of hierarchical nanostructure and the continuously conductive framework of the PAni hydrogel.

For biosensors, one of the most important characteristics is the stability of the enzyme immobilization because enzyme is soluble in water, and the long-term overflow of enzyme causes the fast decay of response signal. In this case, the hierarchical 3D network structure and the chemical structure (excessive phosphate group on phytic acid) of PAni hydrogel promote the enzyme immobilization on the hydrogel support in that enzyme may interact with the hydrogel through the interaction between phosphate groups on hydrogel and amine groups on enzyme. Indeed the response signal maintains no noticeable decrease even after the PAni-glucose oxidase electrode was immersed in phosphate buffer solution for 7 d at 4 °C indicating stable immobilization of glucose oxidase on the hydrogel. Note that the enzyme solution was directly dropped on the hydrogel electrode without further immobilization processes. The excellent electrode performance shows that our 3D PAni hydrogel is a promising candidate for biosensors.

In summary, we report a facile synthesis to prepare a highly porous 3D conductive polymer hydrogel using phytic acid, a naturally occurring molecule, as the dopant and the gelator. The as-synthesized PAni hydrogel forms hierarchical 3D nano- and microstructures. It is composed of porous structures across three length scales from the mesh size between polymer chains (a few angstroms to a few nanometers), depending on the degree of swelling, to the gap size (a few hundred nanometers) between branched nanofibers, and larger micron-size pores. Our 3D PAni hydrogel confers superior properties compared to current reported conducting nanostructures, namely: (*i*) ease of patterning, the hydrogel can be readily patterned using existing fabrication techniques such as ink-jet printing; (*ii*) exceptional electronic conductivity, our approach offers a high throughput route in forming a bulk 3D hierarchical structure of conductive polymers without using an insulating matrix; and (*iii*) unprecedented performance as electrodes for supercapacitors and enzyme sensors, our PAni hydrogel electrode showed low electrical impedance, high energy storage capacity, and excellent cycling performance in supercapacitors. It also exhibited fast sensing speed and ultra-high sensitivity in glucose sensors.

When used for electrochemical devices, our PAni hydrogel showed better performance than other PAni-based systems in terms of high speed of electrochemical process and cycle stability. These are attributed to the relatively short diffusion path favoring molecular and ionic transport due to the open channels of 3D hierarchical nanostructures and to the continuous conductive path within the PAni hydrogel network. The conducting polymer hydrogels could facilitate the design of next-generation electronic systems requiring 3D hierarchical nanostructured morphological control. We envision these systems to be highly useful for a broad range of applications such as supercapacitors, lithium batteries, biosensors, biofuel cells, bioelectronics, and medical electrodes.

Materials and Methods

Synthesis of Polyaniline Hydrogel. In a typical synthesis, 0.286 g (1.25 mmol) ammonium persulfate was dissolved in 1 mL DI water (solution A). Solution B was prepared by mixing 0.921 mL (1 mmol) phytic acid (50%, wt/wt in water, Aldrich), 0.458 mL (5 mmol) aniline and 2 mL DI water. The A and B solutions were cooled to 4 °C and then mixed quickly. To remove excess acid and by-products from polymerization, the polyaniline hydrogel was purified by dialysis (dialysis tube, 12,000–14,000 MW cutoff, Fisher Scientific) for 3 d. Thin hydrogel films were purified by immersing in DI water for 24 h. Finally, the dehydrated PAni hydrogel was prepared by allowing it to dry at 60 °C under vacuum. The gelation time was measured by leaning the beaker every 15 s and turning it upside down until it loses fluidity to determine it is finally gelated.

Characterization. The morphologies of the products were examined using field emission SEM (LEO 1530) and TEM (JEM-200CX). FTIR were recorded on a NEXUS 870 spectrophotometer. UV-vis spectra were measured on a Perkin-Elmer LAMBDA-35 UV-vis spectrophotometer. The crystalline morphology was analyzed with powder XRD (ARL X'TRA) using Cu Ka radiation. The contact angle was recorded on a JJC-1 contact-angle analyzer. TGA was measured on TGA/SDTA851 from METTLER TOLEDO. The solution viscosity was measured on a Brookfield Viscometer DV-II+PRO. AFM topographic images were acquired in the tapping mode regime using a Multimode AFM from Veeco Co. The conductivity of the pressed sample pellet at room temperature was measured using a standard four-point-probe method. The conductivity of PAni hydrogel was evaluated by measuring impedance between two-terminal Platinum electrodes within the frequency range of

0.01 Hz $\sim$ 100 KHz (BioLogic VMP3 equipped with EIS board) where the purified PAni hydrogel was put in a glass tube with a length of 32.6 mm and a diameter of 6.8 mm and sandwiched between a pair of platinum electrodes.

Patterning Polyaniline Hydrogel by Ink-jet Printing and Spray Coating. The Stanford logo and dot arrays were ink-jet printed on a glossy ultra premium photo paper (Epson) using an ink-jet printer (Dimatix Materials Printer, DMP-2800) with 16 nozzles. Hydrogel patterns were generated by sequentially depositing A and B solutions. For spray coating, the glass substrate was covered by a patterned PDMS mask, then A and B solutions were sequentially sprayed using an air brush. The film thickness can be controlled by the number of spray cycles.

Electrochemical Characterization of PAni Hydrogel-Based Supercapacitor Electrodes. The electrodes were prepared as follows: carbon cloths (1 cm $\times$ 2 cm, Fuel Cell Earth LLC, MA) used as current collector were immersed in 6 M HNO_3 solution for 24 h followed by washing with water and ethanol, drying for 30 min in vacuum at 60 °C, and 15 min UV-ozone treatment. The solutions A and B were mixed and immediately dropped onto the carbon cloths (projected area of 1 cm $\times$ 1 cm). They let it sit and react for 6 h and finally purified by immersing into 50 mL DI water for 24 h before electrochemical tests.

The electrochemical characterization was carried out based on a three-electrode system using a BioLogic VMP3 potentiostat-galvanostat multi-channel system equipped with an EIS board. Besides the working electrode (PAni coated on carbon cloth), an Ag/AgCl reference electrode (Fisher Scientific) and a Platinum counter electrode (Fisher Scientific) were used in the measurements. CVs were performed in the potential range of -0.2–0.80 V vs. Ag/AgCl reference electrode under a sweep rate of $5 \sim 200$ mV·s^{-1}.

Galvanostatic charge-discharge tests were performed by cycling the voltage from 0 to 0.8 V at various current densities.

PAni Hydrogel/Glucose Oxidase Amperometric Glucose Biosensor. The electrodes were prepared as follows: 5 µL of mixed A and B solutions were dropped on the surface of a platinum electrode (diameter 5 mm, area 0.1963 cm^2) and allowed to polymerize for 10 min. The electrode was subsequently immersed into DI water for 15 min to remove excess ions and then dehydrated at 45 °C for 20 min in air. Fifteen microliters of aqueous solution of glucose oxidase (10 mg/mL, glucose oxidase type II, $\geq 15,000$ units/g solid, Sigma) were dropped onto the PAni film and the PAni was allowed to rehydrate to form a hydrogel.

The electrochemical experiments were performed with a CHI 660B electrochemical workstation (CH Instruments). A two-compartment, three-electrode cell with a sample volume of 50 mL was employed. The platinum electrode and a SCE were used as the counter electrode and the reference electrode, respectively. Amperometric detection was performed under an applied potential of -0.3 V. The solution was continuously stirred during measurements using a magnetic stirring bar at a speed of 250 rpm.

1. Kopecek J (2002) Polymer chemistry—swell gels. *Nature* 417:388–391.
2. Cushing MC, Anseth KS (2007) Hydrogel cell cultures. *Science* 316:1133–1134.
3. Heeger AJ (2001) Semiconducting and metallic polymers: The fourth generation of polymeric materials (Nobel lecture). *Angew Chem Int Ed* 40:2591–2611.
4. Li D, Huang JX, Kaner RB (2009) Polyaniline nanofibers: A unique polymer nanostructure for versatile applications. *Acc Chem Res* 42:135–145.
5. Lee K, et al. (2006) Metallic transport in polyaniline. *Nature* 441:65–68.
6. Wallace GG, Moulton SE, Clark GM (2009) Electrode-cellular interface. *Science* 324:185–186.
7. Peppas NA, Hilt JZ, Khademhosseini A, Langer R (2006) Hydrogels in biology and medicine: From molecular principles to bionanotechnology. *Adv Mater* 18:1345–1360.
8. Green RA, Baek S, Poole-Warren LA, Martens PJ (2010) Conducting polymer-hydrogels for medical electrode applications. *Sci Technol Adv Mater* 11:014107.
9. Guiseppi-Elie A (2010) Electroconductive hydrogels: Synthesis, characterization and biomedical applications. *Biomaterials* 31:2701–2716.
10. Ghosh S, Rasmusson J, Inganas O (1998) Conductivity in conjugated polymer blends: Ionic crosslinking in blends of poly(3,4-ethylenedioxythiophene) poly(styrenesulfonate) and poly(vinylpyrrolidone). *Adv Mater* 10:1097–1099.
11. Ghosh S, Inganas O (1999) Conducting polymer hydrogels as 3D electrodes: Applications for supercapacitors. *Adv Mater* 11:1214–1218.
12. Mano N, Yoo JE, Tarver J, Loo Y-L, Heller A (2007) An electron-conducting cross-linked polyaniline-based redox hydrogel, formed in one step at pH 7.2, wires glucose oxidase. *J Am Chem Soc* 129:7006–7007.
13. Dai T, Jia Y (2011) Supramolecular hydrogels of polyaniline-poly(styrene sulfonate) prepared in concentrated solutions. *Polymer* 52:2550–2558.
14. Samotus B, Schwimmer S (1962) Phytic acid as a phosphorus reservoir in developing potato tuber. *Nature* 194:578–578.
15. Hatch AJ, York JD (2010) Snap shot: Inositol phosphates. *Cell* 143:1030–1031.
16. Li L, et al. (2009) Facile fabrication of uniform core-shell structured carbon nanotube-polyaniline nanocomposites. *J Phys Chem C* 113:5502–5507.
17. Mai L, et al. (2011) Rational synthesis of silver vanadium oxides/polyaniline triaxial nanowires with enhanced electrochemical property. *Nano Lett* 11:4992–4996.
18. Chen L, Kim B, Nishino M, Gong JP, Osada Y (2000) Environmental responses of polythiophene hydrogels. *Macromolecules* 33:1232–1236.
19. Xia Y, Zhu H (2011) Polyaniline nanofiber-reinforced conducting hydrogel with unique pH-sensitivity. *Soft Matter* 7:9388–9393.
20. Mott N, Davis E (1979) *Electronic Processes in Noncrystalline Materials* (Clarendon Press, Oxford), 2nd Ed, p 34.
21. Tian ZRR, Liu J, Voigt JA, Xu HF, McDermot MJ (2003) Dendritic growth of cubically ordered nanoporous materials through self-assembly. *Nano Lett* 3:89–92.
22. Zhang H, Yu X, Braun PV (2011) Three-dimensional bicontinuous ultrafast-charge and -discharge bulk battery electrodes. *Nat Nanotechnol* 6:277–281.
23. Mai LQ, et al. (2011) Hierarchical MnMoO$_4$/CoMoO$_4$ heterostructured nanowires with enhanced supercapacitor performance. *Nat Commun* 2:381.
24. Giri G, et al. (2011) Tuning charge transport in solution-sheared organic semiconductors using lattice strain. *Nature* 480:504–508.
25. Ghosh S (1995) Near-neighbor interactions in protonation of polyaniline. *Macromolecules* 28:4729–4732.
26. Wang JZ, Zheng ZH, Li HW, Huck WTS, Sirringhaus H (2004) Dewetting of conducting polymer ink-jet droplets on patterned surfaces. *Nat Mater* 3:171–176.
27. Hu LB, et al. (2009) Highly conductive paper for energy-storage devices. *Proc Natl Acad Sci USA* 106:21490–21494.
28. Hecht DS, Hu LB, Irvin G (2011) Emerging transparent electrodes based on thin films of carbon nanotubes, graphene, and metallic nanostructures. *Adv Mater* 23:1482–1513.
29. Rudge A, Davey J, Raistrick I, Gottesfeld S, Ferraris JP (1994) Conducting polymers as active materials in electrochemical capacitors. *J Power Sources* 47:89–107.
30. Horng Y-Y, et al. (2010) Flexible supercapacitor based on polyaniline nanowires/carbon cloth with both high gravimetric and area-normalized capacitance. *J Power Sources* 195:4418–4422.
31. Yan Y, Cheng Q, Wang G, Li C (2011) Growth of polyaniline nanowhiskers on mesoporous carbon for supercapacitor application. *J Power Sources* 196:7835–7840.
32. Xu F, et al. (2010) Improving electrochemical performance of polyaniline by introducing carbon aerogel as filler. *Phys Chem Chem Phys* 12:3270–3275.
33. Ryu KS, Kim KM, Park NG, Park YJ, Chang SH (2002) Symmetric redox supercapacitor with conducting polyaniline electrodes. *J Power Sources* 103:305–309.
34. Li H, et al. (2009) Theoretical and experimental specific capacitance of polyaniline in sulfuric acid. *J Power Sources* 190:578–586.
35. Sivakkumar SR, et al. (2007) Electrochemical performance of polyaniline nanofibers and polyaniline/multi-walled carbon nanotube composite as an electrode material for aqueous redox supercapacitors. *J Power Sources* 171:1062–1068.
36. Dhand C, Das M, Datta M, Malhotra BD (2011) Recent advances in polyaniline based biosensors. *Biosens Bioelectron* 26:2811–2821.
37. Forzani ES, et al. (2004) A conducting polymer nanojunction sensor for glucose detection. *Nano Lett* 4:1785–1788.
38. Wang Z, Liu S, Wu P, Cai C (2009) Detection of glucose based on direct electron transfer reaction of glucose oxidase immobilized on highly ordered polyaniline nanotubes. *Anal Chem* 81:1638–1645.
39. Uang YM, Chou TC (2003) Fabrication of glucose oxidase/polypyrrole biosensor by galvanostatic method in various pH aqueous solutions. *Biosens Bioelectron* 19:141–147.
40. Salimi A, Compton RG, Hallaj R (2004) Glucose biosensor prepared by glucose oxidase encapsulated sol-gel and carbon-nanotube-modified basal plane pyrolytic graphite electrode. *Anal Biochem* 333:49–56.
41. Gao QA, Guo YY, Zhang WY, Qi HL, Zhang CX (2011) An amperometric glucose biosensor based on layer-by-layer GOx-SWCNT conjugate/redox polymer multilayer on a screen-printed carbon electrode. *Sensor Actuator B Chem* 153:219–225.